EUROPEAN ORGANIZATION FOR NUCLEAR RESEARCH

CERN-EP/85-89
3 June 1985

EVIDENCE FOR A $\omega\rho^{\pm}\pi^{\mp}$ STATE IN DIFFRACTIVE PHOTOPRODUCTION

Omega Photon Collaboration

M. Atkinson[7], T.J. Axon[5], D. Barberis[5], T.J. Brodbeck[4], G.R. Brookes[8], J.J. Bunn[8], P.J. Bussey[3], A.B. Clegg[4], J.B. Dainton[3], M. Davenport[7], B. Dickinson[5], B. Diekmann[1], A. Donnachie[5], R.J. Ellison[5], P. Flower[7], P.J. Flynn[4], W. Galbraith[8], K. Heinloth[1], R.C.W. Henderson[4], R.E. Hughes-Jones[5], J.S. Hutton[7], M. Ibbotson[5], H.-P. Jakob[1], M. Jung[1], B.R. Kumar[7], J. Laberrigue[6], G.D. Lafferty[5], J.B. Lane[5], J.-C. Lassalle[2], J.M. Lévy[6], V. Liebenau[1], R.H. McClatchey[8], D. Mercer[5], J.A.G. Morris[7], J.V. Morris[7], D. Newton[4], C. Paterson[3], G.N. Patrick[2], E. Paul[1], C. Raine[3], M. Reidenbach[1], H. Rotscheidt[1], A. Schlösser[1], P.H. Sharp[7], I.O. Skillicorn[3], K.M. Smith[3], K.M. Storr[2], R.J. Thompson[5], Ch. de la Vaissière[6], A.P. Waite[5], M.F. Worsell[5] and T.P. Yiou[6]

Bonn[1]-CERN[2]-Glasgow[3]-Lancaster[4]-Manchester[5]-Paris VI[6]-Rutherford[7]-Sheffield[8]

ABSTRACT

The photoproduction of the final state $\omega\pi^+\pi^-\pi^0$ has been studied as part of a survey of photoproduction in the energy range 20–70 GeV in the Omega Spectrometer at CERN. The $\pi^+\pi^-\pi^0$ system produced with the ω meson has a strong $\rho^{\pm}\pi^{\mp}$ component which is predominantly $I = 1$ and $J^{\pi} = 1^+$. For the $\omega\rho^{\pm}\pi^{\mp}$ state a spin-parity analysis favours $J^{\pi} = 1^-$, and the mass spectrum peaks at 2.28 ± 0.05 GeV. The fitted width is $\Gamma = 0.44 \pm 0.11$ GeV. The photoproduction cross-section of the $\omega\rho^{\pm}\pi^{\mp}$ state, averaged over the energy range 25–60 GeV, is 150 ± 50 nb.

(Submitted to Zeitschrift für Physik C)

0022P/DN/sm

1. Introduction

In this paper we report on the photoproduction of the state $\pi^+\pi^-\pi^0\pi^+\pi^-\pi^0$. The high energy photoproduction of six pion states has been previously reported only for the state $\pi^+\pi^-\pi^+\pi^-\pi^+\pi^-$, and mainly from the point of view of the jet-like structure of the final state (1). We concentrate in this paper on the particular final state $\omega\pi^+\pi^-\pi^0$ in the reaction

$$\gamma p \rightarrow (p)\, \omega \pi^+\pi^-\pi^0 \qquad (1)$$

The dynamical characteristics of the $\pi^+\pi^-\pi^0$ state produced with the ω meson show that the quantum numbers are largely those which have been reported for the A_1 meson, namely I = 1 and $J^\pi = 1^+$. However no evidence for any narrow peaking in the $\pi^+\pi^-\pi^0$ mass spectrum due to the A_1 meson is found, and this is interpreted as evidence that the width of the A_1 meson is at least 0.2 GeV, in agreement with other recent observations (2),(3).

The selection of events analysed here favours the production of $\omega\pi^+\pi^-\pi^0$ states produced with the quantum numbers of the incident photon. The data do indeed support the hypothesis C=-1 for the $\omega\pi^+\pi^-\pi^0$ state, indicated by strong $\rho^\pm$ production within the $\pi^+\pi^-\pi^0$ system opposite the ω meson, but no ρ^0 production. The mass spectrum of $\omega\rho^\pm\pi^\mp$ states shows a broad peak at approximately 2.3 GeV.

2. Experiment and Data Sample

This analysis was made as part of the WA57 experiment, in which an 80 GeV electron beam from the CERN SPS was used to produce tagged photons of energy 20-74 GeV. The tagged photon beam was incident on a 60 cm liquid hydrogen target, and the secondary particles produced were detected in the Omega spectrometer and in a large aperture photon detector. (fig.1).

Charged particles from reactions in the hydrogen target were detected in a system of multiwire proportional chambers inside the magnetic volume of the Omega spectrometer, and drift chambers at the exit from this volume.

The photon calorimeter comprised an active converter (sampler) made up of 42 slabs of lead glass each of 3 radiation lengths in depth, followed by a shower position detector hodoscope of 792 scintillation counters, and finally an array of 343 lead glass blocks, each of area 140 x 140 mm and depth 550 mm (20 radiation lengths). This calorimeter subtended a solid angle of 0.07 sr about the forward direction, and measured the photon direction to an accuracy of $\pm$ 0.6 mrad with an energy resolution given by $\left(\frac{\sigma}{E}\right)^2 = (0.03)^2 + 0.01\, E^{-1}$ where E is the gamma ray energy in Gev.

Events from reaction (1) were selected by a trigger which required between two and five forward charged particles plus a signal from the photon calorimeter indicating the detection of at least one gamma ray of energy above 2 GeV. Electromagnetic background was reduced by a system of veto counters in the

median plane, consisting of the median row blocks of the lead glass array plus additional electron veto counters (EVA's); see fig.1. Pattern recognition and geometrical reconstruction of events were performed by the program TRIDENT (4). A second program reconstructed the momentum of the incident photons, decoded the Cerenkov information for particle identification, and reconstructed π^o mesons from the detected gamma rays.

The experimental acceptance of the apparatus was studied by means of a Monte Carlo programme in which each individual part of the experiment, trigger condition and analysis of the photon detector was realistically simulated. It was found that for the reaction reported here the main effects of apparatus acceptance were through the requirement of two identified π^o mesons in the photon detector.

Events for further analysis were selected as those in which

(i) four or five charged particles consistent with $\pi^+\pi^-\pi^+\pi^-$ or with $p\pi^+\pi^-\pi^+\pi^-$ were observed in the Omega spectrometer, and four gamma rays which could be paired to form two π^o mesons were observed in the photon detector,

(ii) the tagged-photon system recorded a well-measured photon,

(iii) the longitudinal momentum balance between the incident photon and the six pions (and also the recoil proton when detected) was within ± 1.5 GeV.

With these selections the events were from the elastic reaction $\gamma p \to (p)\pi^+\pi^-\pi^0\pi^+\pi^-\pi^0$, with an estimated inelastic background of less than 25 percent.

3. Mass Spectra

The data sample contained 6278 events corresponding to a cross section averaged over the energy range 20-70 GeV, of 800 ± 270 nb, the uncertainty originating from systematic effects. The six-pion mass spectrum when corrected for experimental acceptance is shown in fig.2a. The experimental acceptance falls considerably with increasing six-pion mass greater than approximately 3 GeV. For this reason the further analysis is confined to the 3127 events for which the acceptance is large (of order 0.1) i.e. $1.8 \leq m_{6\pi} \leq 3.4$ GeV. For each of these events all $\pi^+\pi^-\pi^0$ mass combinations were formed (8 entries per event) and fig.2b presents the $\pi^+\pi^-\pi^0$ mass spectrum, which shows a clear ω meson signal, indicating approximately 0.4 ω per event. There is no significant η meson signal.

Further analysis studies the $\pi^+\pi^-\pi^0$ mass combination opposite the ω meson by the following procedure; any combination for which the $\pi^+\pi^-\pi^0$ mass is in the region 753 to 813 MeV is known as an "ω peak" entry, any combination for which the $\pi^+\pi^-\pi^0$ mass is in one of the regions 723 to 753 MeV or 813 to 843 MeV is known as an "ω wings" entry. Entries in spectra were given weight +1 for "ω peak" and -1 for "ω wings", and zero if the $\pi^+\pi^-\pi^0$ combination in question had a mass outside the range 723 to 843 MeV. A mass spectrum for the $\pi^+\pi^-\pi^0$ system opposite the ω meson was obtained in this way, and is shown in

fig.2(c).

The $\pi^+\pi^-$ spectrum in the $\pi^+\pi^-\pi^0$ opposite the ω meson is shown in fig.3(a). The spectra obtained are consistent with those calculated (the curve shown) on the assumption of a decay $X \rightarrow \omega\pi^+\pi^-\pi^0$ according to phase space, with a mass distribution for X taken from the observed $\omega 3\pi$ mass spectrum.

The $\pi^+\pi^0$ and $\pi^-\pi^0$ spectra (added) in the $\pi^+\pi^-\pi^0$ opposite the ω meson are shown in figs.3(b). The spectra obtained are not consistent with those calculated according to the phase space assumptions described in the previous paragraph; a clear $\rho^\pm$ meson peak is evident. The ratio of ρ^+ to ρ^- (not shown) was found to be consistent with one.

The strength of the $\rho^\pm$ in the $\pi^+\pi^-\pi^0$ system opposite the ω meson has been investigated in separate ranges of 0.2 GeV of six-pion mass, by fitting the corresponding $\pi^\pm\pi^0$ mass spectra with

$$\alpha\, x(m) + \beta\, y(m)$$

where m is the $\pi^\pm\pi^0$ mass,

x(m) is a mass spectrum representing the rho meson, for the (fixed) standard mass and width of the rho,

and y(m) is a mass spectrum from a phase space calculation for $X \rightarrow \omega\pi^+\pi^-\pi^0$. Good fits were obtained for each mass bin of the six-pion system. The variation of the estimate α of the $\omega\rho^\pm\pi^\mp$ production as a function of six-pion mass is shown in fig.4(a), and is shown as a fraction of the observed $\omega 3\pi$ ~~mass~~ intensity in fig.4(b). A peaking in the region of 2.3 GeV is observed in the $\omega\rho\pi$ mass spectrum which

is thus narrower than the broad $\omega\pi^+\pi^-\pi^0$ mass spectrum. It has also been checked that effects of acceptance of the apparatus do not produce any significant distortion of the results of fig.4, and in particular do not cause the observed peaking.

A conceivable mechanism for production of $\rho^\pm$ and ω mesons in the $\pi^+\pi^-\pi^0\pi^+\pi^-\pi^0$ final state could be from state X decaying to $B(1235)\rho$. If this state had C = -1 then $B^\pm\rho^\mp$ would occur but not $B^0\rho^0$. This possibility was investigated by examining the $\omega\pi^\pm$ mass spectrum (not shown). No evidence for $B^\pm(1235)$ production was found.

4. The $\pi^+\pi^-\pi^0$ Dalitz plot distribution

Since the $\pi^+\pi^-\pi^0$ system opposite the ω meson contains $\rho^\pm$, but not a ρ^0 meson signal, it must be largely in an I = 1 state, and thus C = +1. Thus C = -1 for the six-pion system of $\omega\pi^+\pi^-\pi^0$, as expected if it is produced by diffractive dissociation of the photon. In order to determine other quantum numbers of the $\pi^+\pi^-\pi^0$ system opposite the ω meson it is necessary to examine the Dalitz plot for the $\pi^+\pi^-\pi^0$ system. For this purpose a further mass selection $2.0 \leq m_{\omega\pi\pi\pi} \leq 2.4$ GeV was made, since fig.4 shows that in this range the fraction of $\omega\rho^\pm\pi^\mp$ rises to 0.5.

The radial distribution of entries in a 3-pion Dalitz plot may be specified by the parameter

$$\lambda = \frac{\left| \underset{\sim}{P_1} \times \underset{\sim}{P_2} \right|^2}{\frac{3}{4}\left[\left(\frac{m_{3\pi}}{3}\right)^2 - m_\pi^2\right]^2}$$

where $\underset{\sim}{p}_1$ and $\underset{\sim}{p}_2$ are the vector momenta of two of the pions in the three pion rest frame.

Natural parity states of the 3-pion system (J^π = 1-,2+,3- ...) have zero density of entries at the boundary, $\lambda = 0$. Thus the λ distribution for the $\pi^+\pi^-\pi^0$ entries opposite the ω meson gives a first indication of the spin-parity of this system. Fig.5 shows this λ distribution; the density shows no sign of approaching zero as $\lambda \to 0$, so natural parity is excluded. This excludes, for example, ωA_2 as an important contributor to the six-pion state being studied here.

As a check on the analysis procedure the λ distribution was examined for the $\pi^+\pi^-\pi^0$ combinations in the ω signal. A good linear rise from the origin was found, as expected for a J^π = 1- state, and as is well established for the ω-meson (5).

The azimuthal distribution of events in the Dalitz plot has been studied because of the opportunity to demonstrate the well-known zero density at the bottom (zero π^0 kinetic energy) of the Dalitz plot for a J^π=1+ and I=1 state of 3 pions (6). For combinations of $\pi^+\pi^-\pi^0$ opposite the ω meson which had $\lambda < 0.333$ and were thus near to the boundary, the angle ψ of the point in the Dalitz plot was calculated, in a convention with ψ = 0 at the top (maximum π^0 kinetic energy). The resulting distribution in the angle ψ is shown in fig.6 where correction has been made for the variation of Dalitz plot area with angle ψ. For comparison fig.6 also shows the expected distribution for this radial band $\lambda < 0.333$ for J^π = 1+ and I =

1, where the proportion of $\rho^{\pm}$ relative to phase space has been chosen to agree with that found for the ratio α/β for the mass range $2.0 < m_{6\pi} < 2.4$ GeV. There is good agreement between experimental and expected distributions ($\chi^2 = 10.2$ for 8 deg. freedom) supporting a hypothesis of $J^{\pi} = 1+$ and $I = 1$ for the $\pi^+\pi^-\pi^0$ system opposite the ω meson. It has been checked that the shape of this angle ψ distribution is not affected by apparatus acceptance.

5. Angular distributions

The Dalitz plot distributions may be supplemented by suitable angular distributions which are affected by the angular momentum state of the $\pi^+\pi^-\pi^0$ system (refered to now as the A system) opposite the ω meson. We have studied the distributions of the angle θ_A between the normal to the A decay plane and the ω meson momentum vector, in the rest frame of the A system, and the angle θ_ω between the normal to the ω decay plane and the A momentum vector, in the rest frame of the ω meson. We have also studied the angle ϕ between the normals to the ω decay plane and to the A decay plane, projected onto the plane normal to the ω A line of flight. The observed angular distributions are shown in fig.7. The curves shown will be described below.

Within the range $2.0 \leq m_{6\pi} \leq 2.4$ GeV the $\pi^+\pi^-\pi^0$ state opposite the ω is 0.5 $\rho^{\pm}\pi^{\mp}$ and 0.5 phase space. The phase space contribution gives flat distributions in $\cos\theta_A$, $\cos\theta_\omega$ and ϕ, and the expected distributions from the $\rho^{\pm}\pi^{\mp}$ contribution have been calculated as follows. For a

given $(J^{\pi})_{\omega A}$ of the ωA system, the decay into ω + A may occur with orbital angular momentum $\underset{\sim}{\ell}$, and channel spin $\underset{\sim}{S} = \underset{\sim}{S}_{\omega} + \underset{\sim}{S}_{A}$ with $(\underset{\sim}{J})_{\omega A} = \underset{\sim}{\ell} + \underset{\sim}{S}$. Taking the A to be 1+, the angular distributions for θ_A and for θ_ω and for ϕ have been evaluated using wave functions discussed by Berman and Jacob (7) for all possibilities ℓ = 0,1, with S = 0,1,2 and $(J^{\pi})_{\omega A}$ = 0+, 0-, 1+, 1-, 2+, 2-, 3+. The distributions are of the forms

$$1 + k_A \cos^2\theta_A \quad \text{and} \quad 1 + k_\omega \cos^2\theta_\omega \quad \text{and} \quad 1 + k_\phi \cos 2\phi$$

with $k_\omega = \dfrac{-2k_A}{1 + k_A}$ if there is no interference between channel spin states.

Figure 7 shows the results of simultaneous fits to the θ_A and θ_ω and ϕ distributions, and table 1 shows the chisquared values for the fits. Each calculated shape contains a 50% phase space contribution. Spin-parities for the ωA system which are disfavoured by poor fits are 0- and 0+. The best fit for any single channel spin is obtained for $(J^{\pi})_{\omega A}$ = 1-, ℓ = 0, S = 1. The possibilities $(J^{\pi})_{\omega A}$ = 1+, 2-, 2+, 3+ cannot be excluded; although the single channel spins give poorer fits than for 1- the opportunity for particular interfering conspiracies allow 1+ and 2+ to give fits of comparable quality but in a rather contrived way. The curves drawn in fig.7 illustrate the best fitting single channel spins for each of the possibilities $(J^{\pi})_{\omega A}$ = 0+, 0-, 1+, 1-, 2+, 2-, 3+.

These angles θ_A, θ_ω, ϕ are internal to the $\omega\pi^+\pi^-\pi^0$ system. Angular distributions with respect to external axes, such as the s-channel helicity axis, yield no reliable information because (i) the effects of apparatus acceptance and (ii) the complexity of possibly interfering amplitudes make interpretation less certain than for the internal angles discussed.

6. Other features of the data

A study of the $\pi^+\pi^-\pi^0$ system opposite the ω meson favours I=1, C=-1, J^π = 1+ for this $\pi^+\pi^-\pi^0$ system. One thus has the conditions in which the A_1 meson should be expected to show as a $\rho\pi$ final state interaction. The $\pi^+\pi^-\pi^0$ mass spectrum opposite the ω meson has been studied, comparing the observed spectrum with that calculated for various assumed masses and widths of the A_1 meson, truncated by phase space. A mass less than 1.2 Gev and a width less than 0.2 Gev was found to be inconsistent with the data ; however precise determinations of mass and width are precluded because the $\pi^+\pi^-\pi^0$ mass spectrum is insensitive to the A_1 parameters when the assumed width is greater than 0.2 Gev. These conclusions on mass and width are in complete agrement with the results obtained by Daum et al. (2) and by Dankowych et al. (3).

As noted in section 3 there is little or no photoproduction of $\eta\pi^+\pi^-\pi^0$ in the data selected as described in section 2. This selection may be expected to favour events resulting from diffractive dissociation of the photon ; if one assumes C = -1 for the diffractively produced 6π state, then the G = -1

state of $\eta 3\pi$ would have to come from the isoscalar part of the photon, whereas the G = +1 state of $\omega 3\pi$ can come from the isovector part of the photon. This can explain the dominance of $\omega 3\pi$ over $\eta 3\pi$. We note that in a previous study of the photoproduction of 5π states, $\eta 2\pi$ production was found to be approximately equal to that of $\omega 2\pi$ (γ). In that case the G = +1 state of $\eta 2\pi$ comes from the isovector part of the photon, and the G = -1 state of $\omega 2\pi$ from the isoscalar part.

The cross section for photoproduction of the $\omega\rho^{\pm}\pi^{\mp}$ state has been evaluated after correcting for inefficiencies in the analysis programmes, experimental inefficiences in certain counters, and branching ratio of ω mesons to 3π. We find σ = 150±50 nb, averaged over the energy range 25-60 GeV. The energy dependence of this cross section, after correction for acceptance, falls with incident photon energy as $E^{-1.5 \pm 0.25}$ as shown in fig.8. Although this dependence is somewhat steeper than has been found for other diffractive dissociation processes, it is to be expected that the dependence steepens as the mass increases, as has been indicated in other reactions (9).

The angular distributions described in section 5 support the interpretation in terms of diffractive dissociation of the photon into a $(J^{\pi})_{\omega A}$ = 1- state, which then undergoes s-wave decay to ω and $\rho^{\pm}\pi^{\mp}$ in a 1+ state. If fig 4a is interpreted as a resonant effect of ω and $\rho\pi$, and fitted with a simple Breit-Wigner shape, a mass m = 2.28 ± 0.05 GeV is obtained, and a width Γ = 0.44 ± 0.11 GeV.

7. Summary

Within the reaction $\gamma p \rightarrow (p)\pi^+\pi^-\pi^0\pi^+\pi^-\pi^0$ there is strong production of $\omega\pi^+\pi^-\pi^0$ states. Within the $\pi^+\pi^-\pi^0$ system opposite the ω meson there is a $\rho^\pm$ meson signal but no ρ^0 meson signal, indicating that the $\omega\pi^+\pi^-\pi^0$ system has C = -1, as would be expected for diffractive dissociation of the photon.

The production of the $\omega\rho^{\pm\mp}\pi$ state is strong only for six-pion masses from 2.0 to 2.4 GeV. There is evidence from Dalitz plot distributions that the $\rho^{\pm\mp}\pi$ state has I = 1 and $J^\pi = 1+$, but no narrow $\rho\pi$ state is seen in the mass spectrum, showing that any significant A_1 contribution to the $\rho^{\pm\mp}\pi$ state is possible only if the A_1 width is greater than 0.2 GeV. The angular distributions described in section 5, support the hypothesis that the $\omega\pi^+\pi^-\pi^0$ state is photoproduced by the diffractive dissociation of the photon and is in a $J^\pi = 1-$ state, followed by predominantly s-wave breakup to ω and $\rho\pi$. This 1- state is consistent with two interpretations, a high mass vector meson, or an s-wave threshold enhancement ; the present data are unable to distinguish between these. It may be noted that if the state is a high mass vector meson then the $\rho(760)$, $\rho'(1600)$ and this state are approximately equally spaced in mass squared.

We are grateful to the Omega group at CERN for their help in maintaining and running the spectrometer and providing on-line and off-line software. The work of the technical support staff in our home institutions, and the support at the computer centres at the Rutherford Appleton Laboratory, CERN, and the RHRZ at Bonn have been invaluable. We thank the SERC (UK), the BMFT (Fed. Rep. Germany), and the IN2P3 (France) for financial support.

REFERENCES

1) D. Aston et al., Nucl. Phys. B166 (1980) 1.

2) C. Daum et al., Nucl. Phys. B187 (1981) 1.

3) J.A. Dankowych et al., Phys. Rev. Lett. 46 (1981) 580.

4) J.-C. Lassalle, F. Carena and S.Pensotti, Nucl. Instrum. Methods 176 (1980) 371.

5) S.M. Flatte et al., Phys. Rev. 145 (1966) 1050.

6) C. Zemach, Phys. Rev. B140 (1965) 97.

7) S.M. Berman and M. Jacob, Phys. Rev. 139 (1965) 1023.

8) D. Aston et al., Nucl. Phys. B174 (1980) 269.

9) D. Aston et al., Nucl. Phys. B189 (1981) 15.

Table 1

$(J^\pi)_{\omega A}$	ℓ	S	χ^2	χ^2(interference)	d.o.f.
0-	0	0	18.2		13
0+	1	1	22.5		13
1-	0	1	7.0		13
1+	1	0	18.2		
	1	1	11.0	5.8	11
	1	2	14.8		
2-	0	2	9.9		13
2+	1	1	7.2		
				7.0	12
	1	2	17.1		
3+	1	2	10.0		13

Figure captions

1. The Omega spectrometer, and the photon detector used for π^0 detection in this experiment.

2. (a) the mass spectrum, corrected for acceptance of the $\pi^+\pi^-\pi^0\pi^+\pi^-\pi^0$ events.

   (b) the mass spectrum of $\pi^+\pi^-\pi^0$ combinations (8 per event) for events in which $1.8 \leqslant m_{6\pi} \leqslant 3.4$ GeV (corresponding to high acceptance).

   (c) the mass spectrum of the $\pi^+\pi^-\pi^0$ combination opposite the ω combination.

3. (a) the mass spectrum of $\pi^+\pi^-$ in the $\pi^+\pi^-\pi^0$ combination opposite the ω combination.

   (b) the combined mass spectrum of $\pi^+\pi^0$ and $\pi^-\pi^0$ in the $\pi^+\pi^-\pi^0$ combination opposite the ω combination. The dotted curves are explained in the text.

4. (a) The number of fitted $\omega\rho^{\pm}\pi^{\mp}$ events as a function of six pion mass.

(b) the fraction of $\omega\pi^+\pi^-\pi^0$ events which are fitted as $\omega\rho^\pm\pi^\mp$ events, as a function of six pion mass.

5. The radial distribution of Dalitz plot entries for the $\pi^+\pi^-\pi^0$ combinations opposite the ω combination. The distribution has been corrected for a small dependence of acceptance on the position in the Dalitz plot.

6. For $\pi^+\pi^-\pi^0$ combinations opposite the ω combination, and which have $\lambda < 0.333$, the azimuthal angle from the top ($\psi = 0$) of the Dalitz plot is shown. The dotted curve is explained in the text.

7. Distributions of three correlated angles in the ωA system, where A denotes the $\pi^+\pi^-\pi^0$ combination opposite the ω.

θ_A is defined in the A rest frame as the angle between the normal to the A decay plane and the ω direction.

θ_ω is defined in the ω rest frame as the angle between the normal to the ω decay plane and the A direction.

ϕ is the (projected) angle between the normals to the ω and A decay planes, as described in the text.

The curves show the best fits for several possible quantum number combinations, as explained in the text, when a simultaneous fit is

made to the θ_A and θ_ω and ϕ distributions.

8. The cross section for photoproduction of $\omega\rho^{\pm}\pi^{\mp}$ events, as a function of incident photon energy.

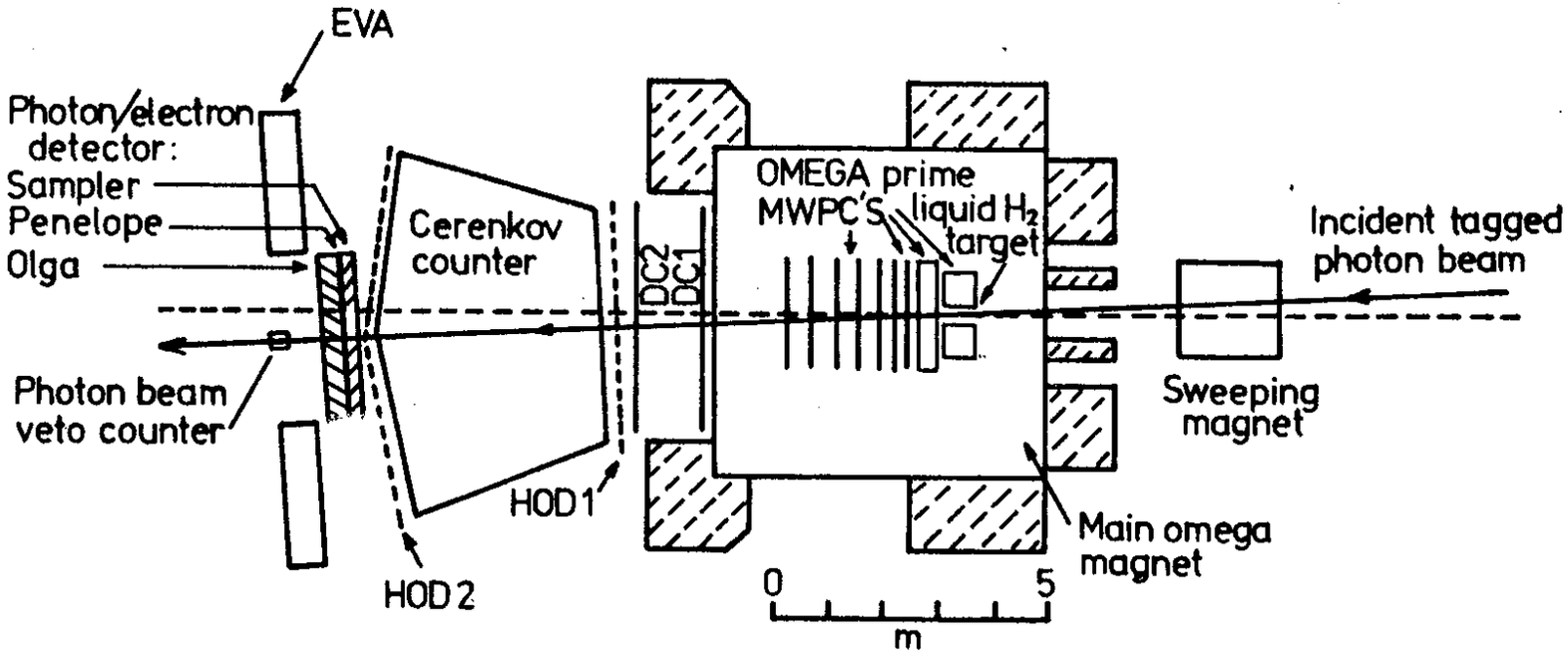
EVA
Photon/electron detector:
Sampler
Penelope
Olga
Photon beam veto counter
HOD 2
Cerenkov counter
HOD 1
DC2
DC1
OMEGA prime MWPC'S
liquid H_2 target
Incident tagged photon beam
Sweeping magnet
Main omega magnet
0
5
m

Fig. 1

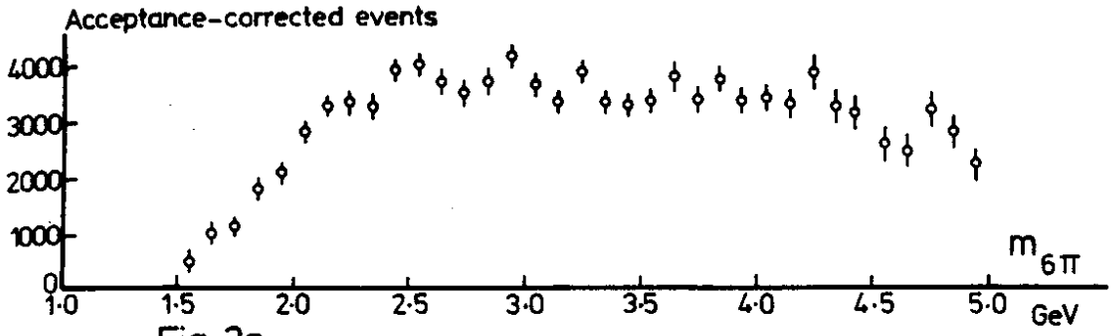

Fig. 2a

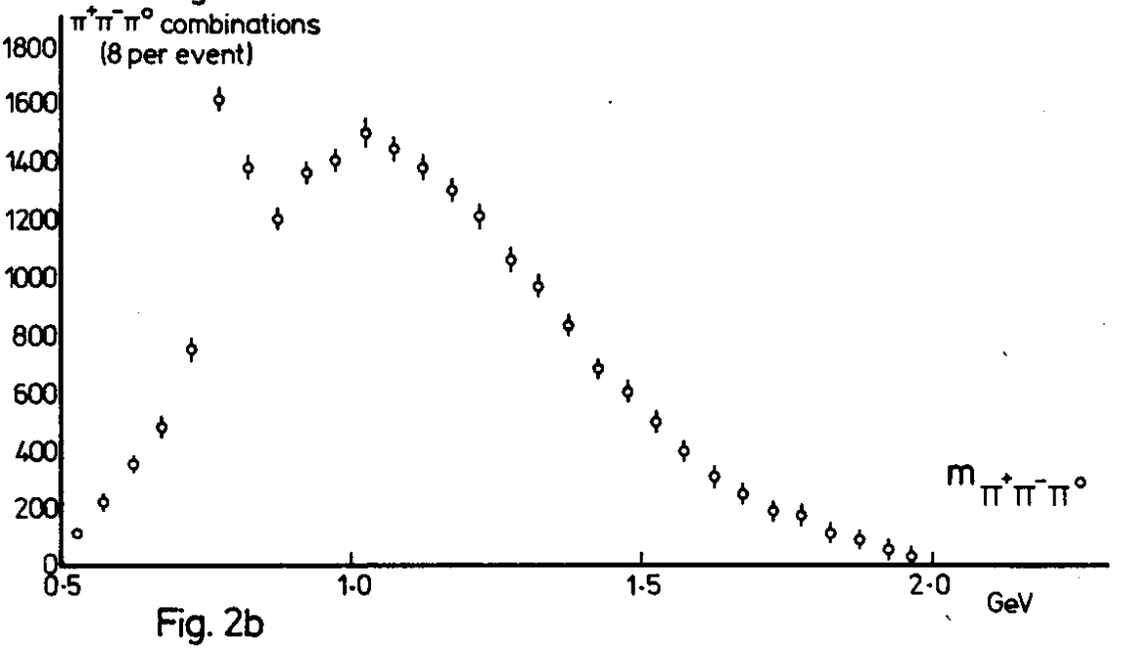

Fig. 2b

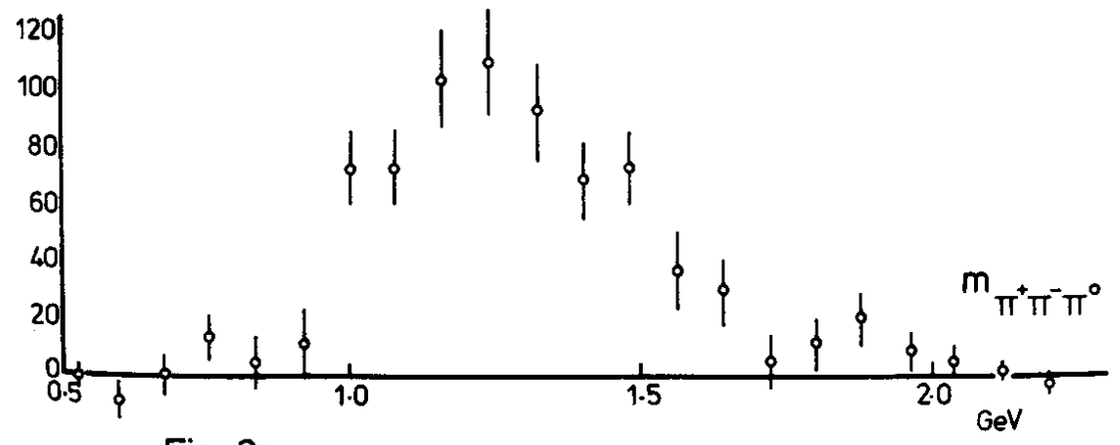

Fig. 2c

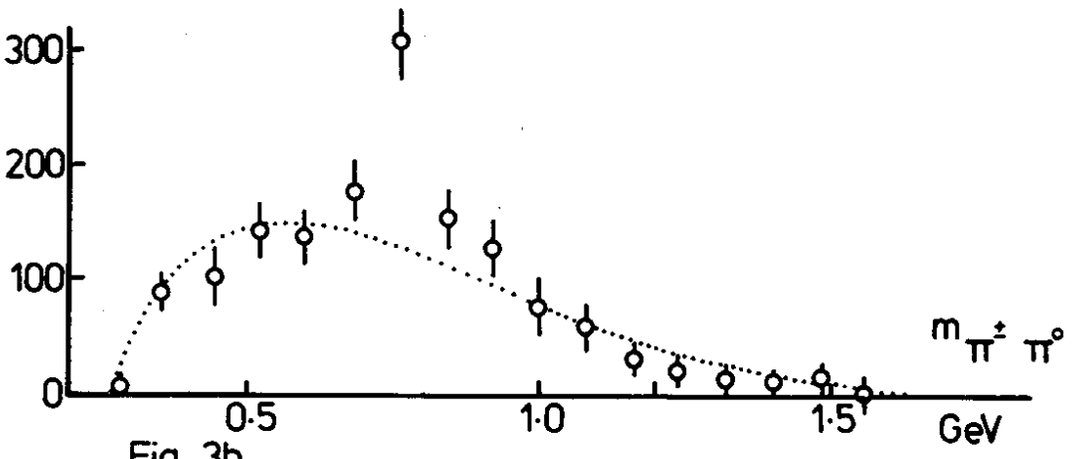
300
200
100
0
0·5
1·0
1·5
GeV
$m_{\pi^{\pm}\pi^{0}}$

Fig. 3b

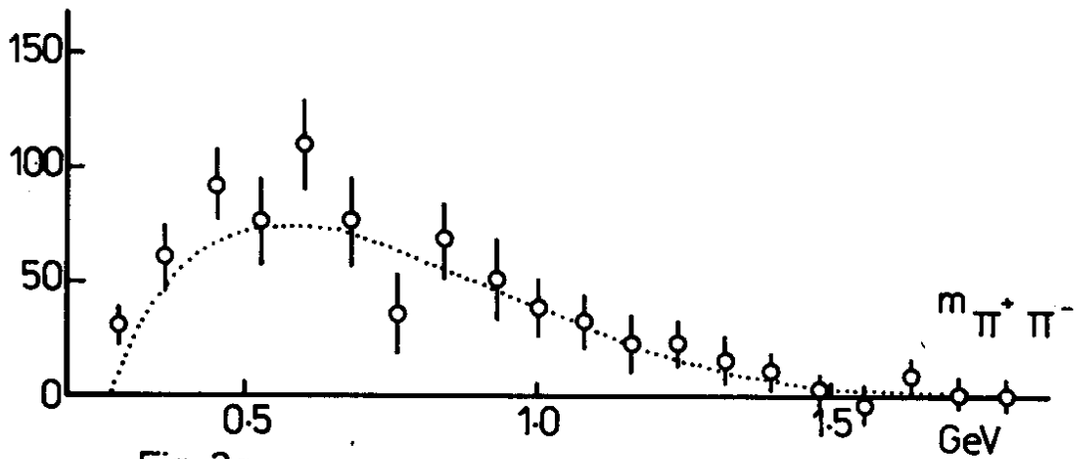
150
100
50
0
0·5
1·0
1·5
GeV
$m_{\pi^{+}\pi^{-}}$

Fig. 3a

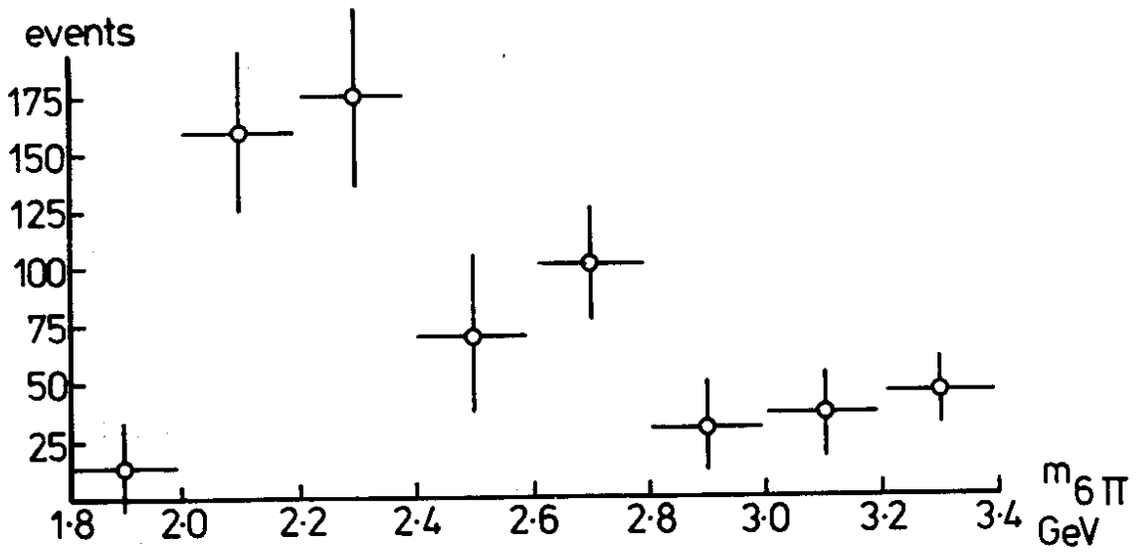
events
175
150
125
100
75
50
25
1·8
2·0
2·2
2·4
2·6
2·8
3·0
3·2
3·4
$m_{6\pi}$
GeV

Fig. 4a

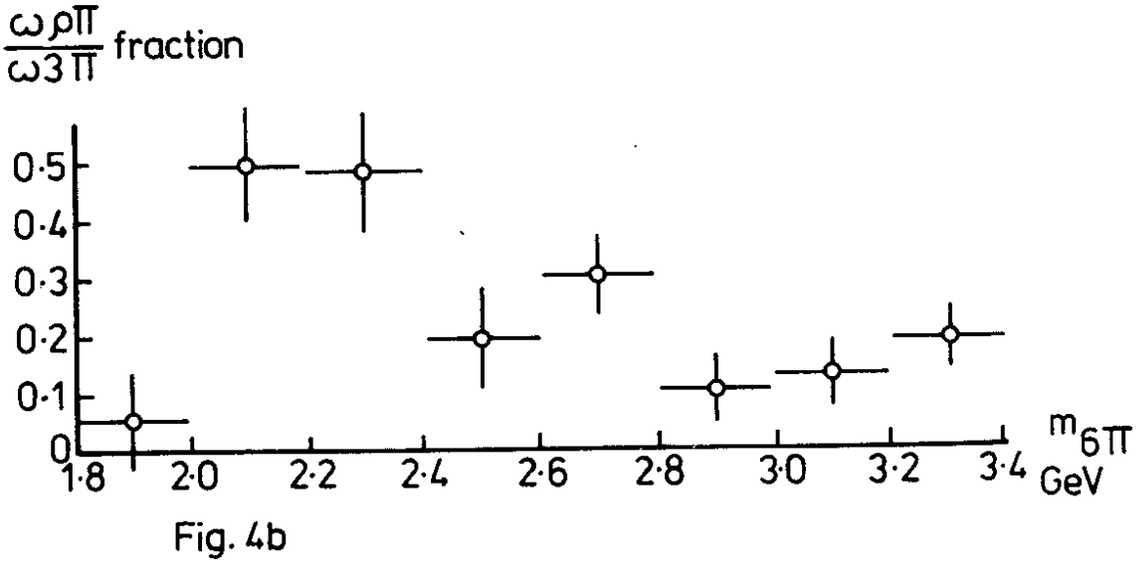
$\frac{\omega\rho\pi}{\omega 3\pi}$ fraction
0·5
0·4
0·3
0·2
0·1
0
1·8
2·0
2·2
2·4
2·6
2·8
3·0
3·2
3·4
$m_{6\pi}$
GeV

Fig. 4b

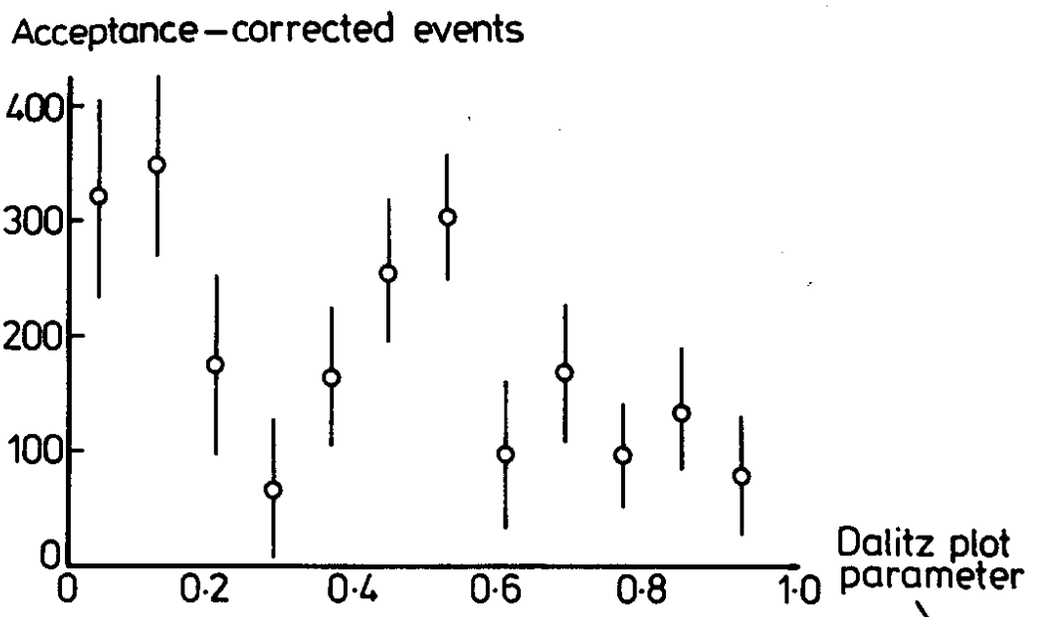
Acceptance–corrected events
400
300
200
100
0
0
0·2
0·4
0·6
0·8
1·0
Dalitz plot parameter
λ

Fig. 5

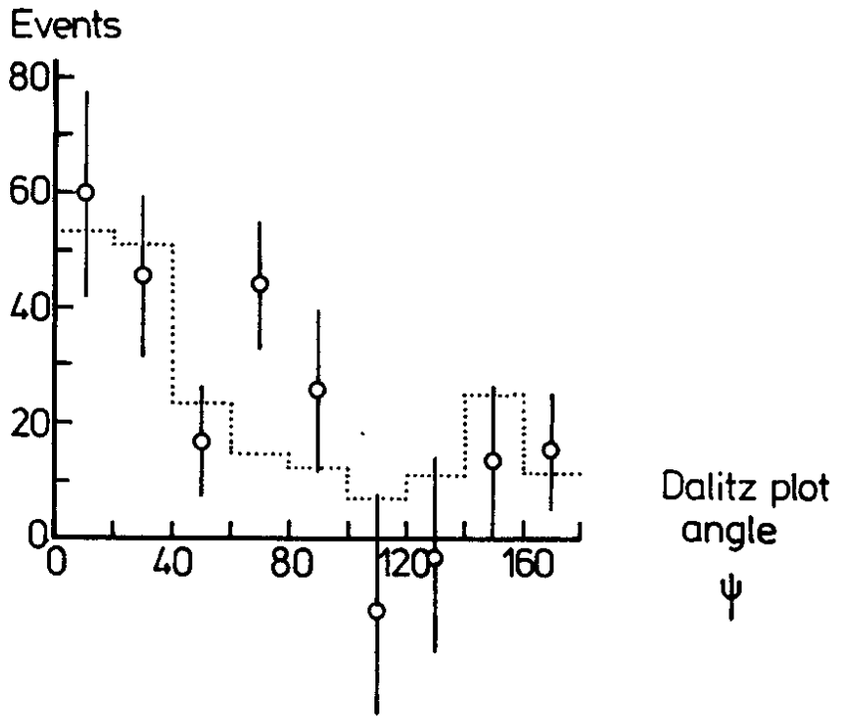
Events
80
60
40
20
0
0
40
80
120
160
Dalitz plot angle
ψ

Fig. 6

Fig. 7

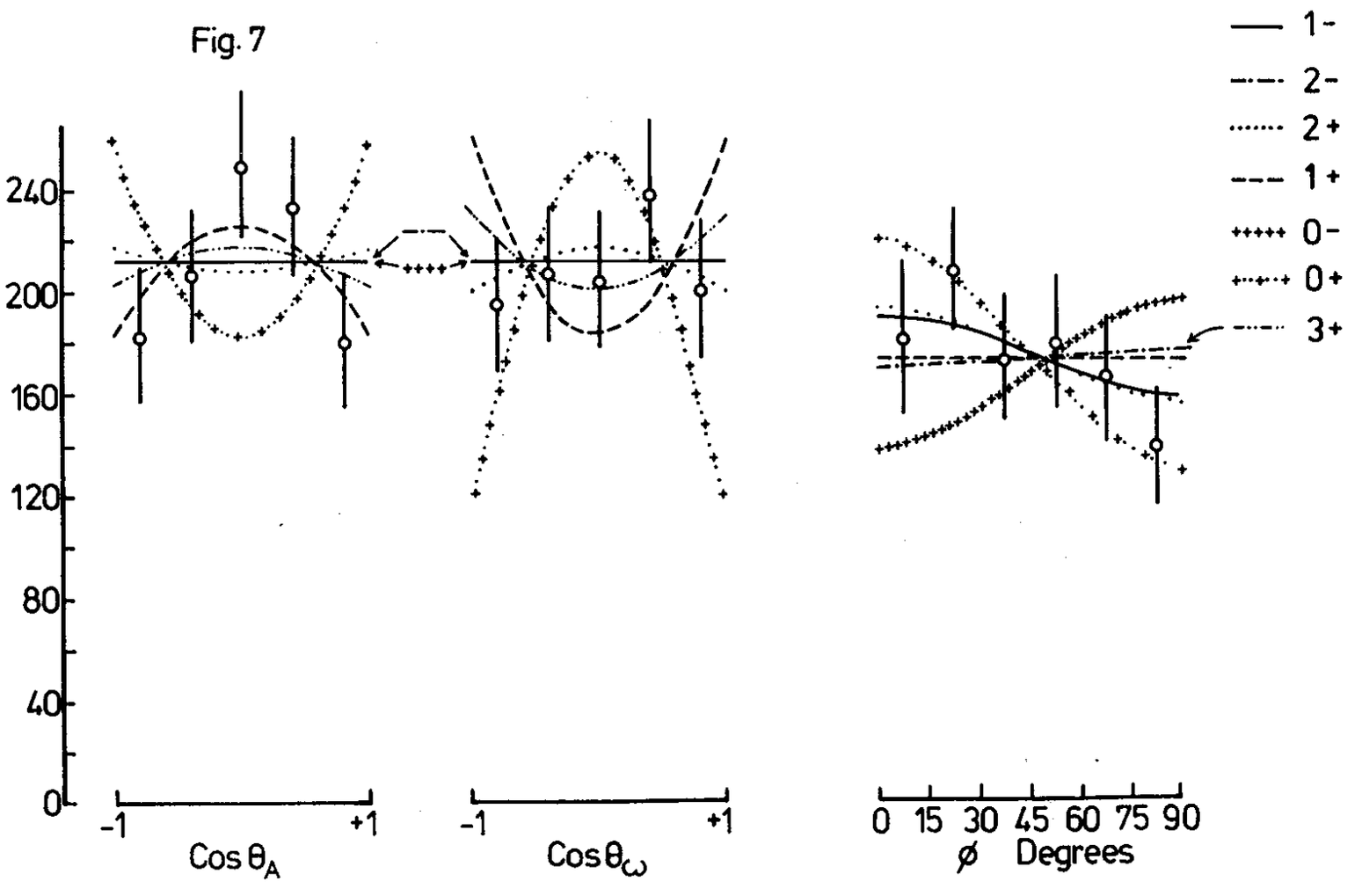
240
200
160
120
80
40
0
-1
+1
Cos θA
-1
+1
Cos θω
0 15 30 45 60 75 90
ø Degrees
1-
2-
2+
1+
0-
0+
3+

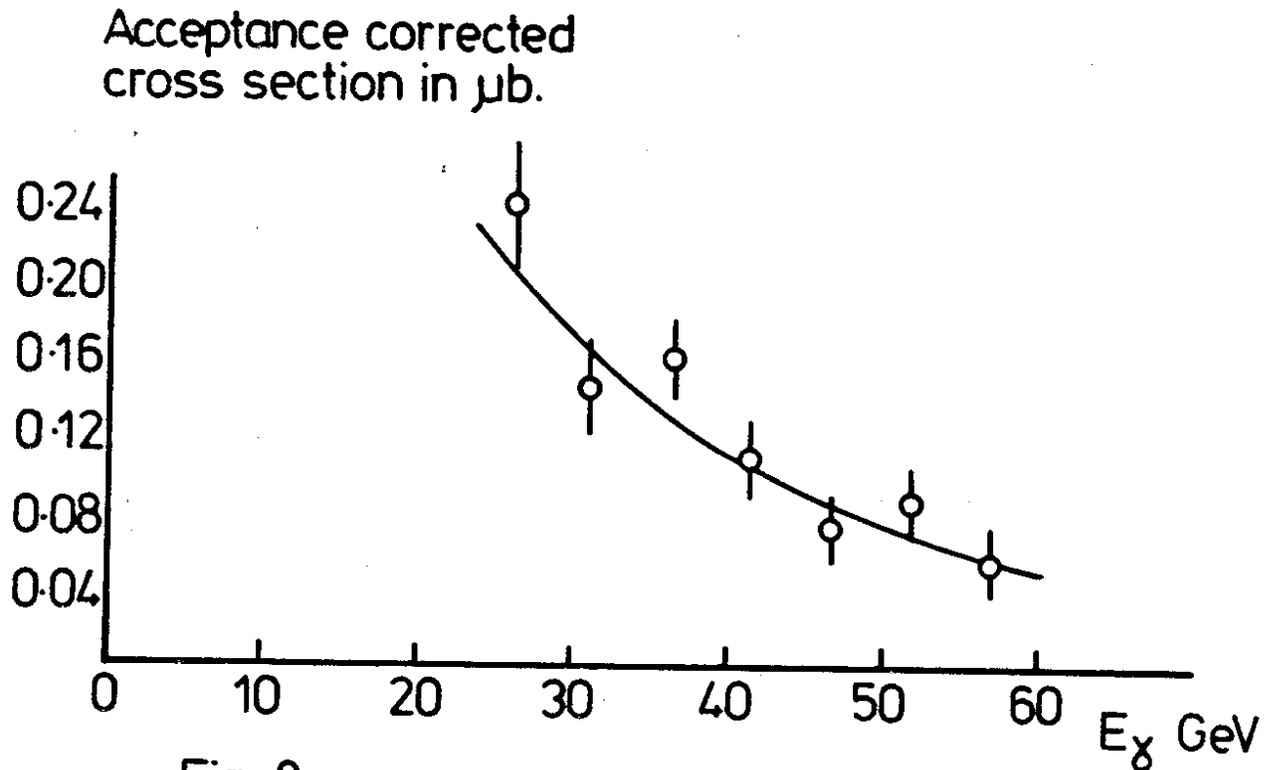
Acceptance corrected
cross section in μb.
0·24
0·20
0·16
0·12
0·08
0·04
0
10
20
30
40
50
60
E_γ GeV

Fig. 8